



HAL
open science

Critical evaluation of climate syntheses to benchmark CMIP6/PMIP4 127 ka Last Interglacial simulations in the high-latitude regions

E. Capron, A. Govin, R. Feng, B.L. Otto-Bliesner, E.W. Wolff

► **To cite this version:**

E. Capron, A. Govin, R. Feng, B.L. Otto-Bliesner, E.W. Wolff. Critical evaluation of climate syntheses to benchmark CMIP6/PMIP4 127 ka Last Interglacial simulations in the high-latitude regions. *Quaternary Science Reviews*, 2017, 168, pp.137 - 150. 10.1016/j.quascirev.2017.04.019 . hal-01584123

HAL Id: hal-01584123

<https://hal.science/hal-01584123>

Submitted on 24 Jun 2021

HAL is a multi-disciplinary open access archive for the deposit and dissemination of scientific research documents, whether they are published or not. The documents may come from teaching and research institutions in France or abroad, or from public or private research centers.

L'archive ouverte pluridisciplinaire **HAL**, est destinée au dépôt et à la diffusion de documents scientifiques de niveau recherche, publiés ou non, émanant des établissements d'enseignement et de recherche français ou étrangers, des laboratoires publics ou privés.

1 **Critical evaluation of climate syntheses to benchmark CMIP6/PMIP4 127 ka Last Interglacial**
2 **simulations in the high-latitude regions.**

3 E. Capron^{1,2}, A. Govin³, R. Feng⁴, B. L. Otto-Bliesner⁴ and E. W. Wolff⁵

4 ¹ Centre for Ice and Climate, Niels Bohr Institute, University of Copenhagen, Juliane Maries Vej 30, DK-2900,
5 Copenhagen, Denmark;

6 ² British Antarctic Survey, High Cross, Madingley Road, Cambridge CB3 0ET, UK;

7 ³ LSCE/IPSL, Laboratoire des Sciences du Climat et de l'Environnement (CEA-CNRS-UVSQ), Université Paris-
8 Saclay, 91190 Gif-Sur-Yvette, France;

9 ⁴ Climate and Global Dynamics Laboratory, National Center for Atmospheric Research (NCAR), Boulder, CO
10 80305, USA;

11 ⁵ Department of Earth Sciences, University of Cambridge, CB2 3EQ Cambridge, UK.

12 Corresponding author: capron@nbi.ku.dk

13 **Abstract:**

14 The Last Interglacial (LIG, ~129-116 thousand years ago, ka) represents an excellent case study to
15 investigate the response of sensitive components of the Earth System and mechanisms of high-latitude
16 amplification to a climate warmer than present-day. The Paleoclimate Model Intercomparison Project (Phase
17 4, hereafter referred as PMIP4) and the Coupled Model Intercomparison Project (Phase 6, hereafter referred
18 as CMIP6) are coordinating the design of (1) a LIG Tier 1 equilibrium simulation to simulate the time slice at
19 127 ka, a time interval associated with a strong orbital forcing and greenhouse gas concentrations close to
20 preindustrial levels and (2) associated Tier 2 sensitivity experiments to examine the role of the ocean,
21 vegetation and dust feedbacks in modulating the response to this orbital forcing.

22 Evaluating the capability of the CMIP6/PMIP4 models to reproduce the 127 ka polar and sub-polar
23 climate will require appropriate data-based benchmarks which are currently missing. Based on a recent data
24 synthesis that offers the first spatio-temporal representation of high-latitude (i.e. poleward of 40°N and 40°S)
25 surface temperature evolution during the LIG, we produce a new 126-128 ka time slab, hereafter named 127
26 ka time slice. This 127 ka time slice represents surface temperature anomalies relative to preindustrial and
27 associated with quantitative estimates of the uncertainties related to relative dating and surface temperature
28 reconstruction methods. It illustrates warmer-than-preindustrial conditions in the high-latitude regions of
29 both hemispheres. In particular, summer sea surface temperatures (SST) in the North Atlantic region were on
30 average 1.1°C (with a standard error of the mean of 0.7°C) warmer relative to preindustrial and 1.8°C (with a
31 standard error of the mean of 0.8°C) in the Southern Ocean. In Antarctica, average 127 ka annual surface air
32 temperature was 2.2°C (with a standard error of the mean of 1.4°C) warmer compared to preindustrial.

33 We provide a critical evaluation of the latest LIG surface climate compilations that are available for
34 evaluating LIG climate model experiments. We discuss in particular our new 127 ka time-slice in the context
35 of existing LIG surface temperature time-slices. We also compare the 127 ka time slice with the ones
36 published for the 125 and 130 ka time intervals and we discuss the potential and limits of a data-based time
37 slice at 127 ka in the context of the upcoming coordinated modeling exercise. Finally we provide guidance on

38 the use of the available LIG climate compilations for future model-data comparison exercises in the
39 framework of the upcoming CMIP5/PMIP4 127 ka experiments. We do not recommend the use of LIG peak
40 warmth-centered syntheses. Instead we promote the use of the most recent syntheses that are based on
41 coherent chronologies between paleoclimatic records and provide spatio-temporal reconstruction of the LIG
42 climate. In particular, we recommend using our new 127 ka data-based time slice in model-data comparison
43 studies with a focus on the high-latitude climate.

44

45 *Key words:* Last Interglacial, 127 ka surface temperature time slice, CMIP6/PMIP4 Tier 1 and Tier 2 simulations,
46 quantitative uncertainty estimates attached to relative dating and temperature reconstruction methods.

47

48 **1. Introduction:**

49 Understanding the climate processes and feedbacks occurring in high-latitude regions is essential for
50 predicting future high-latitude responses to rising atmospheric CO₂ concentrations. These areas are amongst
51 the most affected by global climate change due to their sensitivity to changes in radiative forcing, and they act
52 as amplifiers of climate change through changes in snow and ice cover and associated albedo feedbacks (e.g.
53 Hartmann et al., 2013; Vaughan et al., 2013). The high latitudes provide also the climatic context responsible
54 for polar ice sheet melting and consequently, sea level changes (e.g. DeConto and Pollard, 2016). Besides,
55 surface oceanic conditions (e.g. temperature, salinity) in the Nordic Seas and North Atlantic Ocean play a key
56 role in modulating the intensity of the Atlantic Meridional Overturning Circulation (AMOC), responsible for
57 meridional heat transport and heat and carbon storage in the ocean (e.g. Wunch, 2002). However
58 uncertainties remain in the ability of climate models (1) to correctly capture feedbacks involved in polar
59 amplifications (e.g. Braconnot et al. 2012; Schmidt et al., 2014) and (2) to assess future climate changes in the
60 North Atlantic that will affect the stability of the AMOC (e.g. Sgubin et al., 2017).

61 The Last Interglacial (LIG, ~129-116 thousand years BP, ka; Figure 1) represents an appropriate case
62 study to test the skills of climate models and to assess feedbacks accounting for the amplified high-latitude
63 warmth in a range of temperature changes comparable to present-day and projected changes in the near
64 future. A recent study suggests that LIG peak global mean annual sea surface temperatures (SST) were $0.5 \pm$
65 0.3°C warmer than the preindustrial climatological mean (calculated from 1870 to 1889) but
66 indistinguishable from the 1995 to 2014 climatological mean (Hoffman et al., 2017). Considering that LIG
67 global sea level was up to 6 to 9 m higher-than-today (e.g. Dutton et al., 2015), this warming trend raises
68 further concerns on the response of the high-latitude regions to a globally warmer-than-preindustrial climate
69 and the vulnerability of Greenland and Antarctica to climate change. Processes and feedbacks at play during
70 the LIG are not yet fully understood and in particular large-scale discrepancies currently exist between LIG
71 simulations and reconstructions for the surface temperature trends over the polar and sub polar regions (e.g.
72 Lunt et al., 2013; Bakker et al., 2013; Otto-Bliesner et al., 2013).

73 The Coupled Model Intercomparison Project (CMIP) and Paleoclimate Model Intercomparison Project
74 (PMIP) coordinate climate and paleoclimate modelling activities and evaluate the capability of models used in
75 future climate projections to reproduce past climates (WCRP-Coupled-Model-Intercomparison-Project-
76 Phase-5, 2011, Braconnot et al., 2012). In the framework of both Phase 6 of CMIP (CMIP6) and Phase 4 of
77 PMIP (PMIP4), an experimental protocol for LIG Tier 1 equilibrium simulations referred to as *lig127k* has
78 been prepared recently (Kageyama et al., 2017; Otto-Bliesner et al. 2016). 127 ka was identified as the most
79 appropriate time interval to investigate the impact of a stronger orbital forcing compared to the preindustrial
80 at a time when atmospheric greenhouse gas concentrations were similar to preindustrial levels and the
81 continental configurations were almost identical to modern (Figure 1). It also occurs sufficiently late within
82 the LIG to only bear a limited climate imprint of the melting of the Northern Hemisphere ice sheets during the
83 penultimate deglaciation (Govin et al., 2012; Otto-Bliesner et al., 2016).

84 One of the objectives of this *lig127k* equilibrium simulation is to examine the connections among
85 large scale and regional climate changes leading to changes in land-sea contrast and amplified warming in the
86 high latitudes under a strong orbital forcing context (Otto-Bliesner et al., 2016). To facilitate diagnosis of the
87 Tier 1 *lig127k* equilibrium experiment, Tier 2 sensitivity simulations are also proposed to examine the impact
88 of uncertainties attached to the boundary conditions and the role of the cryosphere, ocean, vegetation and
89 dust feedbacks in modulating the response to this orbital forcing. In particular, one of the sensitivity
90 experiments will explore the climate response to the release of freshwater into the North Atlantic Ocean (due
91 to Northern Hemisphere ice sheet melting) and the role of such freshwater forcing in generating millennial-
92 scale climate changes i.e. changes at a faster scale than what would be expected solely from the insolation
93 forcing (Goelzer et al., 2016; Stone et al., 2016). Full information on the scientific objectives and design of the
94 *lig127k* and associated sensitivity experiments can be found in Otto-Bliesner et al. (2016).

95 Evaluating these model simulations will require the use of appropriate paleoclimatic data syntheses
96 as benchmarks. The syntheses of LIG quantitative climate reconstructions from Turney and Jones (2010) and
97 McKay et al. (2011) have been used previously for climate model evaluation (Lunt et al., 2013; Otto-Bliesner
98 et al., 2013). However, these compilations are attached to several limitations. First, they are based on
99 paleoclimatic records taken on their original timescales, which introduce dating uncertainties of up to 6 ka
100 (Govin et al., 2015). Second, they consist of a compilation of peak warmth values not occurring necessarily at
101 the same time. Indeed, there is much evidence that the LIG warming was not synchronous globally (e.g. Bauch
102 and Erlenkeuser, 2008; Cortese et al., 2007; NEEM-community-members, 2013; Govin et al., 2012; Masson-
103 Delmotte et al., 2010). Thus, the Turney and Jones (2010) and McKay et al. (2011) syntheses do not represent
104 a climate state prevailing at any specific time periods across the LIG, but instead a virtual image on the LIG
105 peak warmth across the globe. As a result and despite their global geographical extent, the Turney and Jones
106 (2010) and McKay et al. (2011) datasets represent inadequate benchmarks for the upcoming *lig127k*
107 simulation and associated sensitivity experiments.

108 We overcame the difficulty of harmonizing chronologies of marine and ice records from different
109 hemispheres using a strategy based on climato-stratigraphic alignments (Capron et al., 2014). We produced a

110 spatio-temporal representation of the LIG climate in the high-latitude regions using annual surface air
111 temperature and summer SST from polar ice and marine records above latitudes of 40°N and 40°S. We also
112 proposed four maps of surface temperature anomalies relative to present-day calculated for 2 ka- time slices
113 centred on 130, 125, 120 and 115 ka. This time-evolving synthesis and associated time-slices provide robust
114 data anchors to evaluate climate model capability in representing LIG processes and feedback mechanisms
115 occurring in polar and sub-polar regions (Capron et al., 2014; Loutre et al., 2014; Stone et al., 2016; Pfeiffer
116 and Lohmann, 2016). Following a similar climato-stratigraphic approach, Hoffman et al. (2017) built recently
117 a compilation of annual sea surface temperature records extending down to the tropics, together with three
118 associated maps of SST anomalies at 129, 125 and 120 ka.

119 Despite those recent progresses, no time slice centred on the 127 ka time interval chosen to run the
120 CMIP5/PMIP4 LIG Tier 1 and Tier 2 experiments is available. Yet, studies have illustrated how crucial it is to
121 compare climate simulations with the appropriate paleo-data time period. For instance, snapshot
122 experiments performed by Otto-Bliesner et al. (2013) with the General Coupled Model (GCM) CCSM3 for the
123 130 ka, 125 ka and 120 ka time intervals, simulate North Atlantic sea surface temperatures (SST) that range
124 from little change relative to preindustrial values for 120 ka to 2 to 6 °C maximum warming for 125 and 130
125 ka. These diverse warming signals simulated at different time intervals could not be evaluated by the LIG
126 peak warmth-centred syntheses such as those from Turney and Jones (2010) and McKay et al. (2011), calling
127 for syntheses at the corresponding time periods. Moreover, a study highlighted that when forced by the 130
128 ka orbital configuration and GHG levels only, the CCSM3 and HadCM3 models could not reproduce the inter-
129 hemispheric asynchrony observed in the surface temperature response at 130 ka (Capron et al., 2014). This
130 observation cannot be drawn without comparing the simulations to the data time slice corresponding to 130
131 ka. Building upon this observation, the model-data mismatch was then resolved when accounting for an
132 additional forcing associated with a freshwater input in the North Atlantic to account for Northern
133 Hemisphere ice sheet melting across the penultimate deglaciation (Stone et al., 2016).

134 In this study, we present a new 126-128 ka (hereafter referred to as 127 ka) time slice of surface
135 temperature anomalies relative to preindustrial based on the Capron et al. (2014) synthesis to assist the
136 assessment of the CMIP5/PMIP4 LIG Tier 1 and Tier 2 simulations in the high-latitude regions. After a brief
137 description of the materials and methods (Section 2), we describe the main climatic features highlighted in
138 the 127 ka time slice and differences with the ones existing for 130 and 125 ka (section 3). Finally, we
139 compare our new 127 ka time slice with other existing LIG data syntheses, evaluating their strengths and
140 limitations. We also discuss the validity of such a data time slice at 127 ka in the context of the upcoming
141 modeling exercise (Section 4).

142 **2. Material and Methods**

143 Full information on the recent LIG climate synthesis is available in Capron et al. (2014). Briefly, we
144 combined 47 surface air and sea surface LIG temperature records with a minimum temporal resolution of 2

145 ka for latitudes above 40°N and 40°S. Surface air temperature records are deduced from ice core water
146 isotopic profiles. Sea surface temperatures (SST) are reconstructed in marine cores from foraminiferal Mg/Ca
147 ratios, alkenone unsaturation ratios or microfossil faunal assemblage transfer functions (Figure 1 and Table
148 S1 from Capron et al., 2014). With a LIG absolute dating uncertainty down to ± 1.8 ka (1σ), the Antarctic Ice
149 Core Chronology 2012 (hereafter referred to as AICC2012; Bazin et al., 2013; Veres et al., 2013) is chosen as
150 the reference age scale for all paleoclimatic records. Marine records are transferred onto AICC2012 by
151 assuming that surface-water temperature changes in the sub-Antarctic zone of the Southern Ocean
152 (respectively in the North Atlantic) occurred simultaneously with air temperature variations above
153 Antarctica (respectively Greenland). Details on the climate record alignments are presented in Capron et al.
154 (2014).

155 We calculate temperature averages for the 126-128 ka interval to account for the record temporal
156 resolution, dating uncertainties and potential delays in climate responses. Instead of using temperature
157 anomalies relative to modern-day as in Capron et al. (2014), we calculate temperature anomalies relative to
158 preindustrial to facilitate comparisons with the LIG Tier 1 simulation for which boundary conditions and
159 forcing will be set relative to preindustrial. For each marine core location, we extracted the preindustrial SST
160 from the HadISST dataset for the 1870-1899 interval (Rayner et al., 2003). For our marine core locations, the
161 gridded NODC WOA98 summer SST dataset (representative of modern-day) is on average 0.1°C warmer than
162 the gridded 1870-1899 HadISST dataset in the North Atlantic region and 0.2°C cooler in the Southern Ocean
163 (see Table S1). Note that HadISST is a statistically blended and interpolated dataset of different
164 measurements, representing optimal SST spatial distributions. Uncertainties associated to the HadISST are
165 not currently available (Rayner et al., 2003). These HadISST values at the marine core sites cannot be tested
166 against in-situ preindustrial SST reconstructions since the paleorecords selected for the LIG synthesis do not
167 have a sufficient resolution to correctly establish the pre-industrial climate. Yet, the HadISST is shown to be
168 consistent with other datasets across overlapping time span, therefore its uncertainties are likely small
169 (Rayner et al., 2003), especially in comparison to the typical error related to the SST reconstructions included
170 in our study. The preindustrial estimate ($-28.8 \pm 0.7^\circ\text{C}$) of the Greenland NEEM ice core site is based on
171 borehole temperature measurements (Masson-Delmotte et al., 2015). In the absence of such reconstructions
172 for the Antarctic sites, the estimates corresponding to the 1870-1899 time interval rely on water isotopic
173 profiles, they are similar to modern instrumental ones within less than 1°C except for EDML (less than 2°C; A.
174 Orsi, personal communication).

175 We calculate 127 ka surface temperature anomalies relative to preindustrial and temperature
176 differences between (1) 127 and 130 ka and (2) 125 and 127 ka, all associated with quantitative uncertainties
177 by following the methodology presented in Capron et al. (2014). Briefly, we apply to both ice core and marine
178 records a Monte Carlo analysis performed with 1000 age model simulations. For each site, it relies on the
179 surface temperature record resampled every 0.1 ka after being transferred onto AICC2012 by linear
180 interpolation between the defined tie points (details in Table S2 from Capron et al., 2014). From 1000 slightly
181 different SST anomalies obtained for the 126-128 ka time windows, we calculated the median 127 ka surface

182 temperature anomaly and associated confidence intervals (2σ) defined by the 2.5th and 97.5th percentiles.
183 These non-parametric uncertainties take into account temperature reconstruction errors and relative dating
184 uncertainties. The 127 ka average uncertainty is $\sim 3.0^\circ\text{C}$ (2σ). Similar procedure is followed to deduce the
185 temperature differences between (1) 127 and 130 ka and (2) 125 and 127 ka, and their respective 2σ
186 uncertainties.

187 Note that originally this approach was not used for ice core records in Capron et al. (2014) and only
188 the uncertainty associated with temperature reconstructions based on water isotopic profiles, i.e. 1.5°C and
189 4°C for Antarctic and Greenland ice core records respectively was provided. Now, time slice surface air
190 temperature and associated 2σ errors are estimated also for ice core-based temperature records following
191 the same Monte-Carlo based-procedure as for SST reconstructions. While EDC, EDML, Vostok and Talos Dome
192 records are not associated with relative dating errors since they were directly used to produce the reference
193 AICC2012 chronology (Bazin et al., 2012; Veres et al., 2012), we consider relative dating uncertainties
194 associated with the transfer of the NEEM and Dome F records onto AICC2012, in addition to temperature
195 reconstruction errors. For the Dome F ice core, we use an updated site temperature reconstruction (Uemura
196 et al., 2012), it leads to differences of only 0.6°C and 0.1°C for the 130 and 125 ka temperature estimates
197 respectively. Published and updated 130, 127, 125, 120 and 115 ka surface temperature estimates and
198 associated 2σ errors are provided in Table S1.

199 We also provide regional mean SST anomalies for the North Atlantic, the Southern Ocean and
200 Antarctica at 130, 127 and 125 (Table 1). Because of the little amount of records available but also the larger
201 dating uncertainties, we prefer to avoid providing average SST anomalies for the Labrador and Norwegian
202 Seas. Also an average value cannot be provided for Greenland since only one quantitative temperature
203 reconstruction (for the NEEM site) is available so far. The North Atlantic and the Southern Ocean average
204 estimates were calculated by averaging anomalies in $8^\circ \times 8^\circ$ boxes after weighting each zonal average by the
205 area of ocean for each latitudinal band. The Antarctic averages were calculated using the same method and
206 grid box resolution. Note that we also apply the same methodology to the 129, 127 and 125 ka SST anomalies
207 from North Atlantic and Southern Ocean sites above 40°N and 40°S respectively presented in the recent
208 Hoffman et al. (2017). Details are given in the Supplementary Material.

209

210 **3. Results**

211 The 127 ka time slice illustrates mostly warmer than preindustrial conditions in both hemispheres
212 (Figure 2). The area-weighted average summer SST warming relative to preindustrial was 1.1°C (with a 0.7°C
213 standard error of the mean, noted SE hereafter) in the North Atlantic and 1.8°C (SE: 0.8°C) in the Southern
214 Ocean (using 14 and 15 reconstructions respectively, Table 1). However, colder than preindustrial conditions
215 are mostly recorded in the Nordic Seas. A Nordic Seas average SST estimate is not proposed here because of
216 the paucity of available records, reduced proxy sensitivity to record low SST variations and large
217 chronological uncertainties (Capron et al., 2014). In Antarctica, the area-weighted average 127 ka annual
218 surface air temperature was 2.2 (SE: 1.4°C) warmer compared to preindustrial (using four records). Only one

219 quantitative surface air temperature reconstruction above Greenland covering unambiguously the LIG is
220 currently available based on the NEEM ice core water isotopic record. It results in a precipitation-weighted
221 temperature estimate warmer by $7.8 \pm 7.9^\circ\text{C}$ (2σ) at 127 ka (NEEM-community-members, 2013), however a
222 value possibly twice as small was suggested through the recent work from Masson-Delmotte et al. (2015).
223 The correct value remains under discussion (Landais et al., 2016).

224 Surface temperature anomaly calculations between 127 and 130 ka and between 125 and 127 ka
225 (Figure 2, Table 1) highlight differences and similarities between the three intervals. North Atlantic summer
226 SST (S-SST) are $5.3 \pm 1.0^\circ\text{C}$ (mean squared error) warmer at 127 ka compared to 130 ka while small
227 differences are observed between 125 and 127 ka ($0.1 \pm 1.0^\circ\text{C}$). In the Southern Ocean, the 127 and 130 ka
228 time slices evidence a relatively similar pattern ($0.1 \pm 1.2^\circ\text{C}$ of temperature difference) and a slight cooling is
229 observed between 127 and 125 ka ($-0.3 \pm 1.2^\circ\text{C}$ difference). Larger differences are calculated for Antarctica
230 with warmer conditions at 127 ka by $0.3 \pm 2.0^\circ\text{C}$ and $0.9 \pm 2.0^\circ\text{C}$ compared to 130 and 125 ka respectively.
231

232 **4. Discussion**

233 **4.1. On the potential remnant imprint of the millennial-scale bipolar seesaw pattern at 127 ka**

234 The hemispheric surface temperature patterns deduced at 127 ka from Capron et al. (2014) are very
235 different compared to those observed at 130 ka in the Capron et al. (2014) time slice (Figure 3). While the
236 North Atlantic and the Southern Ocean are both warmer than preindustrial at 127 ka ($+1.1^\circ\text{C}$ with SE: 0.7°C
237 and $+1.8^\circ\text{C}$ with SE: 0.8°C respectively), at 130 ka, the North Atlantic temperatures are much cooler than
238 preindustrial (-4.2°C with SE: 0.8°C on average) and the Southern Ocean was already warmer than
239 preindustrial ($+1.8^\circ\text{C}$ with SE: 0.9°C on average). The differences for the North Atlantic region are clearly
240 illustrated by the large warming calculated between 130 and 127 ka ($5.3 \pm 1.0^\circ\text{C}$) while only the small climatic
241 difference observed between 125 and 127 ka ($0.1 \pm 1.0^\circ\text{C}$; Table 1). These patterns are the expression of the
242 asynchronous establishment of peak warmth observed between the Northern Hemisphere temperature
243 records and those from the Southern Hemisphere (Figure 1). The LIG temperature peak in the Southern
244 Hemisphere is reached at 129.3 ± 0.9 ka and at 126.4 ± 1.9 ka in the North Atlantic (Capron et al., 2014). This
245 hemispheric asynchrony illustrated best in the 130 ka time slice from Capron et al. (2014) is attributed to
246 dynamics independent from orbital forcing and related to the bipolar seesaw mechanism (Capron et al.,
247 2014). This mechanism is likely related to the disruption of the Atlantic overturning circulation due to
248 freshwater discharges into the North Atlantic (e.g. Govin et al., 2012; Marino et al., 2015; Stone et al., 2016),
249 leading to the northern high latitudes prolonged cold conditions while contributing to the southern high
250 latitudes early warming (Broecker, 1998; Stocker and Johnsen, 2003; Figure 1). Warmer Antarctic conditions
251 at 127 ka compared to 130, 129 and 125 ka illustrate a remnant of the so-called overshoot, a millennial-scale
252 Antarctic temperature peak occurring at the end of the penultimate deglaciation, and identified as a shorter
253 excursion in GHG records (Figure 1). This overshoot is interpreted as a regional response of the bipolar
254 seesaw mechanism (see discussion in Past-Interglacials-Working-Group-of-PAGES, 2016).

255 Because of the overall dating uncertainties of paleoclimatic records (at least 2 ka) and the potential
256 remaining fingerprint of millennial-scale dynamics around 127 ka, the 127 ka data values should thus be
257 treated with care for data-model comparison purpose of *lig127k* Tier 1 simulations. In particular, the excess
258 warmth in Antarctica and more generally, the remnant of the millennial-scale bipolar seesaw imprint in
259 paleo-records at 127 ka might not be simulated in the *lig127k* simulation solely forced by GHG and orbital
260 forcing. However, additional Tier 2 sensitivity experiments will examine the impact of uncertainties in
261 boundary conditions and in particular the role of cryosphere and ocean feedbacks in modulating the orbital
262 forcing response (Otto-Bliesner et al., 2016). A specific Tier 2 sensitivity experiment will help disentangle the
263 orbital vs. millennial-scale climatic variability by implementing in the baseline *lig127k* simulation a persistent
264 freshwater flux of 0.2 Sv into the North Atlantic (details on the experiment design in Otto-Bliesner et al.,
265 2016).

266 Also, potential delays in the response of specific components of the climate system (e.g. vegetation,
267 deep ocean circulation) to the 127 ka radiative and GHG forcing may exist and these aspects require
268 dedicated investigations. The transient behavior of the climate system will be investigated within PMIP4 with
269 transient simulations to be run between 128 and 122 ka (Otto-Bliesner et al., 2016). In addition to the
270 multiple surface temperature time slices that now exist across the LIG, surface temperature time series are
271 also available and provide a comprehensive data base for studying the transient climate evolution of the LIG
272 (Capron et al., 2014; Hoffman et al., 2017).

273

274 **4.2. Comparison of the recent LIG surface temperature syntheses for the high-latitude regions**

275 Producing paleoclimate record syntheses to quantify LIG surface temperature changes is a long-
276 standing goal in paleoclimate research (e.g. CLIMAP-project-members, 1984; CAPE-Last-Interglacial-Project-
277 Members, 2006; Kaspar et al., 2005). Here, we focus on the four latest compilations (Turney and Jones, 2010;
278 McKay et al., 2011; Capron et al., 2014; Hoffman et al., 2017; Figure 2) and provide an evaluation of their
279 strengths and limitations (Table 2). First we discuss the similarities and differences in terms of temperature
280 reconstructions at 127 ka (Table 3) between the two LIG peak warmth-centered syntheses and our new 127
281 ka time slice (Section 4.1.1.). Second, we provide a more in-depth comparison between the recent Hoffman et
282 al. (2017) synthesis and our 127 ka time slice (Section 4.1.2.). Finally, we provide guidance on the use of these
283 various LIG compilations for future model-data comparisons in the framework of the CMIP6/PMIP4 127 ka
284 experiments (Section 4.1.3.).

285

286 **4.2.1. Comparing our 127 ka time slice with the two LIG peak warmth-centered syntheses**

287 The Turney and Jones (2010) synthesis has the largest spatial coverage and is currently the only
288 synthesis integrating terrestrial records, however this synthesis is associated with four major limitations. (1)
289 It relies on paleoclimatic records taken on their original timescales. (2) It represents a virtual image of the LIG
290 peak warmth conditions but it does not represent a realistic climate for any given time interval during the LIG
291 as it considers implicitly a synchronous maximum warmth across the globe. (3) SST records are all

292 interpreted as annual means and Greenland maximum warmth estimates should be considered with caution
293 (Table 2). (4) Quantitative uncertainties integrating errors on age models, analysis and the calibration of
294 microfossil transfer functions are not provided. The McKay et al. (2011) compilation focuses on the global
295 ocean. Their global mean SST anomalies account for the errors attached to SST tracers, the seasonality of the
296 SST records and for the limited spatial range of paleoclimatic records. However, their synthesis is also
297 centered on the LIG peak warmth and deduced from SST records taken on their original timescales. Also, only
298 a limited number of SST records is included for the high latitudes compared to the other syntheses (Figure 3).

299 We now provide a comparison of the two peak warmth-centered compilations with our 127 ka time
300 slice deduced from Capron et al. (2014). The compiled sites in McKay et al. (2011) do not exhibit the
301 pronounced overall warmth in the North Atlantic observed in Turney and Jones (2010) and in our 127 ka
302 time slice. In addition, the Turney and Jones (2010) synthesis does not illustrate the regional cooling
303 prevailing in the Nordic Seas and in the West North Atlantic at 127 ka. In Table 4, we attempt to compare
304 quantitatively the two peak warmth-centered compilations with the 127 ka time-slice. Such an exercise is
305 challenging mainly because (1) temperature records from different sites are included from one synthesis to
306 the other and (2) different time-intervals are used as references for temperature anomaly calculations. We
307 extract SST values from 13 marine sites that were included in Capron et al. (2014) and in either Turney and
308 Jones (2010; four sites in common) or McKay et al. (2011; three sites in common), or in both syntheses (six
309 sites in common between the three syntheses). For each site, we calculate the difference between the
310 provided peak warmth anomaly value and the 127 ka anomaly. To estimate the overall and regional degree of
311 agreement of each of these peak-warmth syntheses with our 127 ka time slice at these common sites we
312 calculate the resulting Root Mean Standard Deviation (RMSD) considering 1) all sites, 2) the North Atlantic
313 sites only and 3) the Southern Ocean sites only.

314 For a given site, the offset between the value extracted from Turney and Jones (2010) and the 127 ka
315 value varies between -2.8°C and $+8.9^{\circ}\text{C}$. When considering the 10 sites in common between Turney and Jones
316 (2010) and our 127 ka time slice, the RMSD is 3.4°C . It is likely due to the fact that at 127 ka, peak warmth
317 conditions are not systematically already reached in the North Atlantic region (the RMSD including only the
318 six North Atlantic sites is 4.0°C while the RMSD including the four Southern Ocean sites is 1.9°C , see also
319 discussion in section 4.3). Note that we made the same calculation considering the 127 ka values relative to
320 the World Ocean Atlas 1998 instead of a preindustrial reference and the resulting North Atlantic RMSD is
321 3.2°C (not shown). As a result, the large offsets cannot be fully explained by the fact that the time interval of
322 reference chosen for the two syntheses is different. For a given site, the difference between the value from
323 McKay et al. (2011) and the 127 ka value varies between -2.2°C and $+3.9^{\circ}\text{C}$. Overall, the discrepancies are
324 reduced between the McKay et al. (2010) synthesis and our 127 ka time slice but they are still large especially
325 in the North Atlantic region (total RMSD of 1.7°C based on nine sites and of 2.3°C when considering only the
326 three North Atlantic sites). This comparison exercise is somewhat fictional since the Turney and Jones (2010)
327 and McKay et al. (2011) do not represent any particular time interval across the LIG and instead a snapshot
328 on the LIG peak warmth. Still, it enables to illustrate that these two peak warmth-centered syntheses do not

329 represent robust data benchmarks in the North Atlantic and Southern Ocean regions in the framework on the
330 CMIP6/PMIP4 127 ka simulations.

331

332 **4.2.2. Comparing our 127 ka time slice with the most recent Hoffman et al. (2017) compilation**

333 Recently, Hoffman et al. (2017) published a new LIG SST compilation of global extent and associated
334 with a coherent temporal framework and quantitative estimates of the errors combining SST tracers and
335 dating uncertainties (Table 2). Using the data provided in the Supplementary Online Material of Hoffman et al.
336 (2017), we extracted a subset of their synthesis for the high latitudes at 127 ka following the methodology
337 they used for building the 129, 125 and 120 ka time slices (Figure 3). Briefly we took for each core the SST
338 value corresponding to the age 127 ka on the mean 0.1-ka interpolated SST curve resulting from their
339 Bayesian approach which integrates 1000 realizations of SST curves resulting from the propagation of
340 uncertainties associated with age markers and the proxy-based SST calibrations. Surface temperature
341 anomaly was then deduced by using the HadlSST1.1 1870-1889 values provided in the supplementary
342 material of Hoffman et al. (2017).

343 Overall, a comparable number of high-latitude SST records is included in Hoffman et al. (2017) and
344 Capron et al. (2014) but the latter includes in addition polar surface air temperature records from ice cores.
345 The two SST datasets are somehow complementary since Capron et al. (2014) provide mostly summer SST
346 records (40 summer and two annual SST reconstructions) and Hoffman et al. (2017) gather 17 summer and
347 22 annual SST records. However differences in methodologies to define the common temporal framework
348 and to estimate surface temperature changes prevent us to propose a 127 ka time slice combining directly
349 both syntheses (see further discussion below). The two syntheses have 12 summer SST records in common.
350 The difference in site selection in both compilations likely arises from (1) different minimum temporal
351 resolution cuts to select the SST records (2 ka in Capron et al. (2014) and 4 ka in Hoffman et al. (2017)) and
352 (2) a climate alignment strategy in Hoffman et al. (2017) that requires benthic foraminifera $\delta^{18}\text{O}$ record
353 which might not systematically be available in some of the sites selected in Capron et al. (2014).

354 Both syntheses highlight the hemispheric asynchronous pattern in surface temperatures at the
355 beginning of the LIG as observed in the 129 ka time slice from Hoffman et al. (2017) and the 130 ka time slice
356 from Capron et al. (2014) (Figure 3). This observation further supports the crucial need for time-evolving
357 syntheses across the LIG. We now provide a quantitative comparison of the 127 ka time slices inferred from
358 Hoffman et al. (2017) and from our data synthesis following the same method as the method used to compare
359 our 127 ka time slice with the ones from Turney and Jones (2010) and McKay et al. (2011) (Section 4.1.1,
360 Table 3). Such a comparison is more straightforward in the present case since we are able here to use
361 absolute surface temperature values given in the supplementary materials of Hoffmann et al. (2017) and
362 Capron et al. (2014) so that the comparison is not affected by possible differences in preindustrial reference
363 values. The resulting North Atlantic and Southern Ocean RMSD are of 1.2 and 0.8°C respectively. Overall, the
364 resulting RMSD of 1.1°C based on 12 common SST records is much smaller than the RMSD values inferred

365 when comparing our time slice with the LIG peak warmth syntheses and it is also within the range of stated
366 quantitative 2σ uncertainties for both syntheses.

367 Considering that Capron et al. (2014) and Hoffman et al. (2014) use the exact same original SST
368 datasets on a depth scale for these selected sites, we interpret the temperature differences recorded at 127 ka
369 and ranging between 0.1 to 2.0 °C for the different sites in Table 3 as resulting from three main factors. (1)
370 Capron et al. (2014) use AICC2012 (Bazin et al., 2012; Veres et al., 2012) as the reference chronology while
371 Hoffman et al. (2017) use the SpeleoAge time scale which results from the adjustment of the ice core EDC3
372 timescale using radiometric dates from Chinese speleothems (Barker et al., 2011). An offset of about 1 ka is
373 observed between the two time scales around 127 ka, it increases through time reaching up to 3.4 ka around
374 115 ka (Figure 4). (2) The definition of the tie points and associated relative uncertainty, which influence the
375 determination of the final age model and thus the resulting 127 ka temperature values, are different. (3)
376 Despite a similar approach based on a Monte-Carlo analysis with 1000 age model realizations, the two studies
377 do not use the same method of calculation to deduce the age model for each site, as well as quantitative
378 estimates of associated uncertainties. The methodology of Hoffman et al. (2017) is based on Bayesian
379 statistics (Haslett and Parnell, 2008) and results in a greater smoothing of the SST changes on an age scale
380 compared to those inferred with our methodology based on linear interpolation between tie-points. This is
381 illustrated in Figure 4 with a comparison of the resulting dated surface temperature records for the North
382 Atlantic site EW9302-8JPC (Oppo et al., 1997; Oppo et al., 2001) that show an offset of 2°C at 127 ka. This
383 exercise of comparison shows how critical age models, and the way they are defined, are in LIG data
384 compilations. Using different SST interpolation and smoothing scheme also potentially leads to changes in the
385 timing of the LIG maximum warmth and thus to changes in the estimated amplitude of the SST temperature
386 change. As a result, the Capron et al. (2014) and Hoffman et al. (2017) climate syntheses cannot be merged
387 unless a thorough work on harmonizing the chronologies of both compilations is carried out first.

388

389 **4.2.3. Recommendations**

390 Overall, we do not recommend the use of the peak warmth-centered syntheses from Turney and
391 Jones (2010) and McKay et al. (2011) as benchmarks for the 127 ka climate above polar ice sheets and at the
392 surface of the North Atlantic and Southern Oceans in the CMIP6/PMIP4 127 ka simulations. For model-data
393 comparison exercises focused on surface ocean changes at a global scale, a 127 ka time slice of global-scale
394 inferred from the Hoffman et al. (2017) compilation should be favored over the McKay et al. (2011) synthesis
395 changes at a global scale recorded in the ocean. For studies focusing on the high-latitudes regions, we
396 recommend the use of the 127 ka time-slice based on the Capron et al. (2014) as it gather not only the largest
397 number of SST records but also provide information about climatic changes above the polar ice sheets.
398 Finally, the surface temperature records included in Capron et al. (2014) and Hoffman et al. (2014) cannot be
399 combined in their current state.

400

401 **4.3. Regional and global surface temperature averages from LIG climate syntheses**

402 We discuss here new regional and existing global SST averages available across the LIG. While site-
403 specific estimates provide detailed information about the spatial structure of the changes, regional averages
404 provide first order estimate of mean responses across the LIG. Because of potential local bias affecting SST
405 reconstructions and/or potential misrepresentation of processes at local scale in the CMIP6/PMIP4 models,
406 they are particularly useful to evaluate models capability at a global and regional scale and also to benchmark
407 models with reduced spatial resolution.

408 Because (1) air temperature estimates represent precipitation-weighted and annual signals for
409 Greenland and Antarctica respectively, and (2) SST records are mostly interpreted as summer signals, we
410 cannot propose a realistic 127 ka high latitude average surface temperature encompassing all records in our
411 data synthesis. Instead, we propose regional temperature anomalies for the North Atlantic, the Southern
412 Ocean (summer averages) and Antarctica (annual average) at 125, 127 and 130 ka (Table 1) based on records
413 on coherent chronologies and relative to preindustrial. We infer from the Capron et al. (2014) dataset that
414 North Atlantic and Southern Ocean summer averages were +1.1°C (SE: 0.7°C, based on 14 records) and +1.8°C
415 (SE: 0.8°C; based on 15 records) respectively at 127 ka. Following the same methodology, we infer also
416 annual and summer North Atlantic and Southern Ocean averages based on the sites poleward 40°N and 40°S
417 included in the Hoffman et al. (2017) datasets. 127 ka North Atlantic and Southern Ocean summer averages
418 were +1.9°C (SE: 1.7°C, based on nine records) and +1.6°C (SE: 0.9°C, based on seven records) respectively
419 while North Atlantic and Southern Ocean annual averages were -0.2°C (SE: 1.4°C, based on nine records) and
420 +2.7°C (SE: 1.0°C, based on 12 records, see footnote of Table 1 regarding this annual average). Despite
421 existing surface temperature differences observed at 127 ka for a given site included in both compilations (c.f.
422 section 4.1.2, Table 2), the North Atlantic and Southern Ocean regional summer averages from the two
423 compilations based on different methodologies to infer a common chronological framework are overall
424 consistent within their stated uncertainties. Combining the annual and summer averages represents useful
425 quantitative information to evaluate (1) the seasonality of climate models in the high-latitude regions and (2)
426 the sensitivity to the high-latitude summer warmth of the polar ice sheets whose melting caused a 6-9m
427 global sea level rise.

428 The warming at 127 ka relative to preindustrial is greater over polar ice sheets (e.g. +2.2°C with SE:
429 1.4°C above Antarctica) compared to the surface layer of the Southern Ocean and the North Atlantic. First, it
430 likely originates from the fact that land areas on average change more rapidly than the ocean (land-sea
431 contrast; e.g. Joshi et al., 2008; Braconnot et al., 2012). Second, it also arises from the polar amplification of
432 surface warming (e.g. Holland and Bitz, 2003; Masson-Delmotte et al., 2006) due to feedbacks related to
433 surface albedo because of changes in land ice and sea ice cover, to ice sheet elevation and to atmospheric
434 processes such as changes in cloud cover (and cloud radiative feedbacks, e.g. Curry et al., 1996) and
435 variations in heat advection (Alexeev et al., 2005).

436 Finally, Hoffman et al. (2017) estimate that global annual SST were only $0.5 \pm 0.3^\circ\text{C}$ warmer-than-
437 preindustrial at 125 ka and a similar value is inferred at 127 ka based on their time-evolving global stack
438 (Supplementary Online Material from Hoffman et al., 2017). In contrast, the high-latitude summer warming

439 was at least 1.1 (SE: 0.7°C) and 1.6 (SE: 0.9°C) warmer-than-preindustrial in the North Atlantic and the
440 Southern Ocean respectively (Capron et al., 2014; Hoffman et al., 2017). The high-latitude warmth compared
441 to preindustrial conditions is compensated globally because of other regions affected by surface changes of
442 smaller amplitude, i.e. the low-latitude SST records gathered in Hoffman et al. (2017) point toward an annual
443 average SST in the tropics (between 23.5°N and 23.5°S) slightly below the preindustrial mean at 127 ka (-0.1
444 ±0.4°C as inferred from Supplementary Online Material from Hoffman et al., 2017). Overall, these results
445 emphasize the existence of considerable regional and seasonal differences in the amplitude of surface
446 temperature changes at 127 ka, and in particular the large response of the high-latitude regions compared to
447 global ocean surface conditions only slightly warmer than preindustrial.

448

449 **5. Summary and outlook**

450 Based on the Capron et al. (2014) compilation, we produce a 127 ka surface temperature time slice
451 relative to preindustrial showing warmer-than-preindustrial conditions in the high latitudes (Table 1; Figure
452 2). Because at 127 ka, (1) the warmest time period can be reconstructed when considering the two high
453 latitude regions and (2) large millennial-scale climate shifts are limited (Figure 1), it represents the most
454 suitable time interval to run the CMIP5/PMIP4 LIG Tier 1 and Tier 2 simulations. Differences in the climatic
455 patterns observed between the 127 ka, 125 and 130 ka time slices inferred from the Capron et al. (2014)
456 synthesis (and also observed between the 127, 125 and 129 ka time slices inferred from the Hoffman et al.
457 (2017) synthesis) strengthen the need to benchmark the Tier 1 and Tier 2 climate snapshot simulations with
458 data from the appropriate 127 ka time interval.

459 We provide an in-depth evaluation of existing LIG climate syntheses and guidance for using them to
460 evaluate climate model simulations. Due to their chronological limitations and their focus on the LIG peak
461 warmth only, we do not recommend the use of the syntheses of Turney and Jones (2010) and McKay et al.
462 (2011) as benchmarks for the CMIP6/PMIP4 127 ka simulations performed in the high-latitude regions. We
463 recommend instead using the new 127 ka surface temperature dataset. Associated with summer SST
464 reconstructions, it will be particularly useful to evaluate data-model temperature differences seasonally in
465 the context of a large summer insolation forcing in the North Hemisphere. Site-specific estimates provide
466 detailed information about the spatial structure of the changes and the regional averages provide first-order
467 estimates of mean responses at 127 ka.

468 The Turney and Jones (2010) compilation is the only one including continental records. Thus, the fact
469 that it does not represent any specific nor realistic time window should be kept in mind when using it for
470 model-data comparison exercises over land or when using as a benchmark its global annual surface
471 temperature estimate of +1.5 ±0.1°C relative to the 1961-1990 interval. Hoffmann et al. (2017) dataset
472 represents currently the only global ocean synthesis associated with harmonized chronologies extending to
473 the low latitude annual ocean surface temperatures and it should be favored over the McKay et al. (2011)
474 synthesis when investigating LIG SST changes at a global scale.

475 It is common practice to evaluate simulations of present-day climate to multiple observation datasets
476 considered independently because of different blending methods and assimilation systems. In the same way
477 and because of the use of different reference chronologies and methodologies to infer temporal surface
478 temperature changes, the Capron et al. (2014) and Hoffman et al. (2017) datasets should not be combined as
479 such but, instead, treated as independent data benchmarks. Overall, our critical evaluation of available
480 climate syntheses for benchmarking upcoming CMIP6/PMIP4 LIG simulations at 127 ka calls for the urgent
481 need to develop millennial-scale transient climate syntheses of global extent, integrating ice, marine and
482 continental records in a coherent temporal framework accounting for age and tracer uncertainties. In
483 addition, future syntheses should also extend temperature synthesis to additional parameters such as deep
484 ocean circulation changes and sea ice extent.

485 The LIG is not a direct analogue to future climate due to differences in the primary forcing of the
486 warming i.e. caused by larger boreal summer insolation forcing, and not from enhanced greenhouse gas
487 concentrations. However, the recent quantitative regional reconstructions indicate a warmth in the polar and
488 sub-polar regions of similar amplitudes to the ones that might be reached by 2100, in particular in the context
489 of climate policies that would limit global warming to +1.5°C compared to a preindustrial background state.
490 This leaves the LIG as a particularly relevant target for understanding mechanisms and feedbacks at play, and
491 the polar ice sheet response to such high-latitude warmer climate.

492
493 *Acknowledgments:* We are grateful to members of the PAGES/PMIP Working Group on Quaternary
494 Interglacials (QUIGS) and we thank in particular all participants of the *Warm Extremes* Workshop (November,
495 9-12th 2015, Cambridge, UK) for stimulating discussions. We also thank Anaïs Orsi for useful discussions
496 regarding ice core temperature reconstructions. This work is a contribution to the PAGES/PMIP Working
497 Group on Quaternary Interglacials (QUIGS). E. C. is funded by the European Union's Seventh Framework
498 Programme for research and innovation under the Marie Skłodowska-Curie grant agreement no 600207. B. L.
499 O-B is supported by the U.S. National Science Foundation (NSF) sponsorship of NCAR. R. F. acknowledges the
500 funding of the NSF Arctic System Science. E.W.W. is supported by the Royal Society. This is LSCE contribution
501 n°XX.

502

503 **References:**

504 Alexeev, V.A., Langen, P.L., Bates, J.R., 2005. Polar amplification of surface warming on an aquaplanet in “ghost
505 forcing” experiments without sea ice feedbacks. *Climate Dynamics* 24, 655–666.

506 Bakker, P., Stone, E.J., Charbit, S., Chroger, M., Krebs-Kanzow, U., Ritz, S.P., Varma, V., Khon, V., Lunt, D.J.,
507 Mikolajewicz, U., Prange, M., Renssen, H., Schneider, B., Schulz, M., 2013. Last interglacial temperature
508 evolution - a model inter-comparison. *Climate of the past* 9, 605–619.

509 Barker, S., Knorr, G., Edwards, R.L., Parrenin, F., Putnam, A.E., Skinner, L.C., Wolff, E., Ziegler, M., 2011. 800,000
510 Years of Abrupt Climate Variability. *Science* 334, 347-351.

511 Bauch, H.A., Erlenkeuser, H., 2008. A “critical” climatic evaluation of last interglacial (MIS 5e) records from the
512 Norwegian Sea. *Polar Research* 27, 135-151.

513 Bazin, L., Landais, A., Lemieux-Dudon, B., Toyé Mahamadou Kele, H., Veres, D., Parrenin, F., Martinerie, P., Ritz,
514 C., Capron, E., Lipenkov, V., Loutre, M.-F., Raynaud, D., Vinther, B., Svensson, A., Rasmussen, S.O., Severi, M.,
515 Blunier, T., Leuenberger, M., Fischer, H., Masson-Delmotte, V., Chappellaz, J., Wolff, E.W., 2013. An optimized
516 multi-proxy, multi-site Antarctic ice and gas orbital chronology (AICC2012): 120–800 ka. *Climate of the Past*
517 9, 1715-1731.

518 Braconnot, P., Harrison, S.P., Kageyama, P., Bartlein, P.J., Masson-Delmotte, V., Abe-Ouchi, A., Otto-Bliesner, B.,
519 Zhao, Y., 2012. Evaluation of climate models using palaeoclimatic data. *Nature Climate Change* DOI:
520 10.1038/NCLIMATE1456.

521 Broecker, W.S., 1998. Paleocean circulation during the Last Deglaciation: A bipolar seesaw?
522 *Paleoceanography* 13, DOI - 10.1029/1097PA03707.

523 CAPE-Last-Interglacial-Project-Members, 2006. Last Interglacial Arctic warmth confirms polar amplification
524 of climate change. *Quaternary Science Reviews* 25, 1383-1400.

525 Capron, E., Govin, A., Stone, E.J., Masson-Delmotte, V., Mulitza, S., Otto-Bliesner, B., Sime, L., Waelbroeck, C.,
526 Wolff, E., 2014. Temporal and spatial structure of multi-millennial temperature changes at high latitudes
527 during the Last Interglacial. *Quaternary Science Reviews*, doi: 10.1016/j.quascirev.2014.1008.1018.

528 CLIMAP-project-members, 1984. The Last Interglacial Ocean. *Quaternary Research* 21, 123-224.

529 Cortese, G., Abelmann, A., Gersonde, R., 2007. The last five glacial-interglacial transitions: A high-resolution
530 450,000–year record from the subantarctic Atlantic. *Paleoceanography* 22, PA4203.

531 Curry, J.A., Rossow, W.B., Randall, D., Schramm, J.L., 1996. Overview of Arctic cloud and radiation
532 characteristics. *Journal of climate* 9, 1731– 1764.

533 DeConto, R.M., Pollard, D., 2016. Contribution of Antarctica to past and future sea-level rise. *Nature* 531, 591-
534 597.

535 Dutton, A., Carlson, A.E., Long, A.J., Milne, G.A., Clark, P.U., DeConto, R., Horton, B.P., Rahmstorf, S., Raymo, M.E.,
536 2015. Sea-level rise due to polar ice-sheet mass loss during past warm periods. *Science* 349.

537 Goelzer, H., Huybrechts, P., Loutre, M.F., Fichet, T., 2016. Impact of ice sheet meltwater fluxes on the climate
538 evolution at the onset of the Last Interglacial. *Clim. Past* 12, 1721-1737.

539 Govin, A., Braconnot, P., Capron, E., Cortijo, E., Duplessy, J.-C., Jansen, E., Labeyrie, L., 2012. Persistent
540 influence of ice sheet melting on high northern latitude climate during the early Last Interglacial. *Climate of*
541 *the Past* 8, 483-507, doi:410.5194/cp-5198-5483-2012.

542 Govin, A., Capron, E., Tzedakis, P.C., Verheyden, S., Ghaleb, B., Hillaire-Marcel, C., St-Onge, G., Stoner, J.S.,
543 Bassinot, F., Bazin, L., Blunier, T., Combourieu-Nebout, N., El Ouahabi, A., Genty, D., Gersonde, R., Jimenez-
544 Amat, P., Landais, A., Martrat, B., Masson-Delmotte V., Parrenin, F., Seidenkrantz, M.-S., Veres, D., Waelbroeck,
545 C., Zahn, R., 2015. Sequence of events from the onset to the demise of the Last Interglacial: Evaluating
546 strengths and limitations of chronologies used in climatic archives. *Quaternary Science Reviews* 129, 1-36.

547 Hartmann, D.L., Klein Tank, A.M.G., Rusticucci, M., Alexander, L., Brönnimann, S., Charabi, Y., Dentener, F.,
548 Dlugokencky, E., Easterling, D., Kaplan, A., Soden, B., Thorne, P., Wild, M., Zhai, P.M., 2013. Observations:
549 Atmosphere and Surface. In: *Climate Change 2013: The Physical Science Basis. Contribution of Working*
550 *Group I to the Fifth Assessment Report of the Intergovernmental Panel on Climate Change* [Stocker, T.F., D.
551 Qin, G.-K. Plattner, M. Tignor, S.K. Allen, J. Boschung, A. Nauels, Y. Xia, V. Bex and P.M. Midgley (eds.)].

552 Haslett, J., Parnell, A., 2008. A simple monotone process with application to radiocarbon-dated depth
553 chronologies. *J.R. Stat. Soc.* 57, 399–418. doi:10.1111/j.1467-9876.2008.00623.x.

554 Hoffman, J.S., Clark, P.U., Parnell, A.C., He, F., 2017. Regional and global sea-surface temperatures during the
555 last interglaciation. *Science* 355, 276-279.

556 Holland, M.M., Bitz, C.M., 2003. Polar amplification of climate change in coupled models. *Climate Dynamics* 21,
557 221–232.

558 Joshi, M.M., Gregory, J.M., Webb, M.J., Sexton, D.M.H., Johns, T.C., 2008. Mechanisms for the land/sea warming
559 contrast exhibited by simulations of climate change. *Clim Dyn* (2008) 30, 455–465.

560 Jouzel, J., Masson-Delmotte, V., Cattani, O., Dreyfus, G., Falourd, S., Hoffmann, G., Minster, B., Nouet, J., Barnola,
561 J.-M., Fisher, H., Gallet, J.-C., Johnsen, S., Leuenberger, M., Loulergue, L., Luethi, D., Oerter, H., Parrenin, F.,
562 Raisbeck, G., Raynaud, D., Schilt, A., Schwander, J., Selmo, J., Souchez, R., Spahni, R., Stauffer, B., Steffensen, J.P.,
563 Stenni, B., Stocker, T.F., Tison, J.-L., Werner, M., Wolff, E.W., 2007. Orbital and millennial Antarctic climate
564 variability over the past 800,000 years. *Science* 317, 793-796.

565 Kageyama, M., Albani, S., Braconnot, P., Harrison, S.P., Hopcroft, P.O., Ivanovic, R.F., Lambert, F., Marti, O.,
566 Peltier, W.R., Peterschmitt, J.Y., Roche, D.M., Tarasov, L., Zhang, X., Brady, E.C., Haywood, A.M., LeGrande, A.N.,
567 Lunt, D.J., Mahowald, N.M., Mikolajewicz, U., Nisancioglu, K.H., Otto-Bliesner, B.L., Renssen, H., Tomas, R.A.,
568 Zhang, Q., Abe-Ouchi, A., Bartlein, P.J., Cao, J., Lohmann, G., Ohgaito, R., Shi, X., Volodin, E., Yoshida, K., Zhang, X.,
569 Zheng, W., 2017. The PMIP4 contribution to CMIP6 – Part 4: Scientific objectives and experimental design of
570 the PMIP4-CMIP6 Last Glacial Maximum experiments and PMIP4 sensitivity experiments. *Geosci. Model Dev.*
571 *Discuss.* 2017, 1-33.

572 Kaspar, F., Kuhl, N., Cubasch, U., Litt, T., 2005. A model-data comparison of European temperatures in the
573 Eemian interglacial. *Geophys. Res. Letters*, DOI:10.1029/2005GL022456.

574 Landais, A., Masson-Delmotte, V., Capron, E., Langebroek, P.M., Bakker, P., Stone, E.J., Merz, N., Raible, C.C.,
575 Fischer, H., Orsi, A., Prié, F., Vinther, B., Dahl-Jensen, D., 2016. How warm was Greenland during the last
576 interglacial period? *Clim. Past Discuss.* 2016, 1-27.

577 Loulergue, L., Schilt, A., Spahni, R., Masson-Delmotte, V., Blunier, T., Lemieux, B., Barnola, J.M., Raynaud, D.,
578 Stocker, T.F., Chappellaz, J., 2008. Orbital and millennial-scale features of atmospheric CH₄ over the past
579 800,000 years. *Nature* 453, 383-386.

580 Loutre, M.F., Fichet, T., Goosse, H., Huybrechts, P., Goelzer, H., Capron, E., 2014. Factors controlling the last
581 interglacial climate as simulated by LOVECLIM1.3. *Clim. Past* 10, 1541-1565.

582 Lunt, D.J., Abe-Ouchi, A., Bakker, P., Berger, A., Braconnot, P., Charbit, S., Fischer, N., Herold, N., Jungclaus,
583 J.H., Khon, V.C., Krebs-Kanzow, U., Langebroek, P.M., Lohmann, G., Nisancioglu, K.H., Otto-Bliesner, B.L., Park,
584 W., Pfeiffer, M., Phipps, S.J., Prange, M., Rachmayani, R., Renssen, H., Rosenbloom, N., Schneider, B., Stone, E.J.,
585 Takahashi, E., Wei, W., Yin, Q., Zang, Z.S., 2013. A multi-model assessment of last interglacial temperatures.
586 *Climate of the past* 9, 699-717.

587 Lüthi, D., Le Floch, M., Bereiter, B., Blunier, T., Barnola, J.-M., Siegenthaler, U., Raynaud, D., Jouzel, J., Fischer, H.,
588 Kawamura, K., Stocker, T.F., 2008. High-resolution carbon dioxide concentration record 650,000-800,000
589 years before present. *Nature* 453, 379-382.

590 Marino, G., Rohling, E.J., Rodriguez-Sanz, L., Grant, K.M., Heslop, D., Roberts, A.P., Stanford, J.D., Yu, J., 2015.
591 Bipolar seesaw control on last interglacial sea level. *Nature* 522, 197-201.

592 Masson-Delmotte, V., Kageyama, M., Braconnot, P., Charbit, S., Krinner, G., Ritz, C., Guilyardi, E., Jouzel, J., Abe-
593 Ouchi, A., Crucifix, M., Gladstone, R.M., Hewitt, C.D., Kitoh, A., Legrande, A., Marti, O., Merkel, U., Motoi, T.,
594 Ohgaito, R., Otto-Bliesner, B., Peltier, W.R., Ross, I., Valdes, P.J., Vettoretti, G., Weber, S.L., Wolk, F., 2006. Past
595 and future polar amplification of climate change: climate model intercomparisons and ice-core constraints.
596 *Climate Dynamics* 0930-7575.

597 Masson-Delmotte, V., Schulz, M., Abe-Ouchi, A., Beer, J., Ganopolski, A., Gonzalez, Rouco, J.F., Jansen, E.,
598 Lambeck, K., Luterbacher, J., Naish, T., Osborn, T., Otto-Bliesner, B., Quinn, T., Ramesh, R., Rojas, M., Shao, X.,
599 Timmermann, A., 2013. Information from paleoclimate archives. . In: Stocker, T.F., Qin, D., Plattner, G.-K.,
600 Tignor, M., Allen, S.K., Boschung, J., Nauels, A., Xia, Y., Bex, V., Midgley, P.M. (Eds.), *Climate Change 2013: the*
601 *Physical Science Basis. Contribution of Working Group I to the Fifth Assessment Report of the*
602 *Intergovernmental Panel on Climate Change.* Cambridge University Press, Cambridge, United Kingdom and
603 New York, NY, USA, pp. 383-464 (Chapter 5).

604 Masson-Delmotte, V., Steen-Larsen, H.C., Ortega, P., Swingedouw, D., Popp, T., Vinther, B.M., Oerter, H.,
605 Sveinbjornsdottir, A.E., Gudlaugsdottir, H., Box, J.E., Falourd, S., Fettweis, X., Gallée, H., Garnier, E., Gkinis, V.,
606 Jouzel, J., Landais, A., Minster, B., Paradis, N., Orsi, A., Risi, C., Werner, M., White, J.W.C., 2015. Recent changes

607 in north-west Greenland climate documented by NEEEM shallow ice core data and simulations, and
608 implications for past-temperature reconstructions. *The Cryosphere* 9, 1481-1504.

609 Masson-Delmotte, V., Stenni, B., Blunier, T., Cattani, O., Chappellaz, J., Cheng, H., Dreyfus, G., Edwards, R.L.,
610 Falourd, S., Govin, A., Kawamura, K., Johnsen, S.J., Jouzel, J., Landais, A., Lemieux-Dudon, B., Laurantou, A.,
611 Marshall, G., Minster, B., Mudelsee, M., Pol, K., Röthlisberger, R., Selmo, E., Waelbroeck, C., 2010. Abrupt
612 change of Antarctic moisture origin at the end of Termination II. *Proceedings of the National Academy of*
613 *Sciences*, doi: 10.1073/pnas.0914536107.

614 McKay, N.P., Overpeck, J.T., Otto-Bliesner, B.L., 2011. The role of ocean thermal expansion in Last Interglacial
615 sea level rise. *Geophys. Res. Letters* 38, DOI:10.1029/2011GL048280.

616 NEEEM-community-members, 2013. Eemian interglacial reconstructed from a Greenland folded ice core.
617 *Nature* 493, 489-493, doi:10.1038/nature11789.

618 Oppo, D.W., Horowitz, M., Lehman, S.J., 1997. Marine core evidence for reduced deep water production during
619 Termination II followed by a relatively stable substage 5e (Eemian). *Paleoceanography* 12, 51-63, doi:
620 10.1029/1096PA03133.

621 Oppo, D.W., Keigwin, L.D., McManus, J.F., Cullen, J.L., 2001. Persistent suborbital climate variability in marine
622 isotope stage 5 and Termination II. *Paleoceanography* 16, 280-292.

623 Oppo, D.W., McManus, J.F., Cullen, J.L., 2006. Evolution and demise of the Last Interglacial warmth in the
624 subpolar North Atlantic. *Quaternary Science Reviews* 25(23-24), 3268-3277,
625 doi:10.1016/j.quascirev.2006.3207.3006.

626 Otto-Bliesner, B., Rosenbloom, N., Stone, E., McKay, N.P., Lunt, D.J., Brady, E.C., Overpeck, J.T., 2013. How warm
627 was the Last Interglacial? New model-data comparisons. *Philos Trans A Math Phys Eng Sci*, doi:
628 10.1098/rsta.2013.0097.

629 Otto-Bliesner, B.L., Braconnot, P., Harrison, S.P., Lunt, D.J., Abe-Ouchi, A., Albani, S., Bartlein, P.J., Capron, E.,
630 Carlson, A.E., Dutton, A., Fischer, H., Goelzer, H., Govin, A., Haywood, A., Joos, F., Legrande, A.N., Lipscomb,
631 W.H., Lohmann, G., Mahowald, N., Nehrbass-Ahles, C., Pausata, F.S.R., Peterschmitt, J.Y., Phipps, S., Renssen, H.,
632 2016. The PMIP4 contribution to CMIP6 - Part 2: Two Interglacials, Scientific Objective and Experimental
633 Design for Holocene and Last Interglacial Simulations. *Geosci. Model Dev. Discuss.* 2016, 1-36.

634 Past-Interglacials-Working-Group-of-PAGES, 2016. Interglacials of the last 800,000 years. *Reviews of*
635 *Geophysics* doi:10.1002/2015RG000482.

636 Pfeiffer, M., Lohmann, G., 2016. Greenland Ice Sheet influence on Last Interglacial climate: global sensitivity
637 studies performed with an atmosphere-ocean general circulation model. *Clim. Past* 12, 1313-1338.

638 Rayner, N.A., Parker, D.E., Horton, E.B., Folland, C.K., Alexander, L.V., Rowell, D.P., Kent, E.C., Kaplan, A., 2003.
639 Global analyses of sea surface temperature, sea ice, and night marine air temperature since the late
640 nineteenth century. *J. Geophys. Res.* 108, 4407, doi:4410.1029/2002JD002670.

641 Schmidt, G.A., Annan, J.D., Bartlein, P.J., Cook, B.I., Guilyardi, E., Hargreaves, J.C., Harrison, S.P., Kageyama, M.,
642 LeGrande, A.N., Konecky, B., Lovejoy, S., Mann, M.E., Masson-Delmotte, V., Risi, C., Thompson, D.,
643 Timmermann, A., Tremblay, L.B., Yiou, P., 2014. Using palaeo-climate comparisons to constrain future
644 projections in CMIP5. *Clim. Past* 10, 221-250.

645 Sgubin, G., Swingedouw, D., Drijfhout, S., Mary, Y., Bennabi, A., 2017. Abrupt cooling over the North Atlantic in
646 modern climate models. *Nature Communications* 8.

647 Stocker, T.F., Johnsen, S.J., 2003. A minimum thermodynamic model for the bipolar seesaw. *Paleoceanography*
648 18, 1087.

649 Stone, E.J., Capron, E., Lunt, D.J., Payne, A.J., Singarayer, J.S., Valdes, P.J., Wolff, E.W., 2016. Impact of melt water
650 on high latitude early Last Interglacial climate. *Climate of the Past* 12, 1919-1932.

651 Turney, C.S.M., Jones, R.T., 2010. Does the Agulhas Current amplify global temperatures during super-
652 interglacials? *Journal of Quaternary Science* 25(6), 839–843.

653 Uemura, R., Masson-Delmotte, V., Jouzel, J., Landais, A., Motoyama, H., Stenni, B., 2012. Ranges of moisture-
654 source temperature estimated from Antarctic ice cores stable isotope records over glacial–interglacial cycles.
655 *Clim. Past* 8, 1109-1125.

656 Vaughan, D.G., Comiso, J.C., Allison, I., Carrasco, J., Kaser, G., Kwok, R., Mote, P., Murray, T., Paul, F., Ren, J.,
657 Rignot, E., Solomina, O., Steffen, K., Zhang, T., 2013. Observations: Cryosphere. In: *Climate Change 2013: The*
658 *Physical Science Basis, Contribution of Working Group I to the Fifth Assessment Report of the*
659 *Intergovernmental Panel on Climate Change*, edited by: Stocker, T. F., Qin, D., Plattner, G.-K., Tignor, M., Allen,
660 S.

661 K., Boschung, J., Nauels, A., Xia, Y., Bex, V., and Midgley, P. M., Cambridge University Press, Cambridge, United
662 Kingdom and New York, NY, USA.

663 Veres, D., Bazin, L., Landais, A., Toyé Mahamadou Kele, H., Lemieux-Dudon, B., Parrenin, F., Martinerie, P.,
664 Blayo, E., Blunier, T., Capron, E., Chappellaz, J., Rasmussen, S.O., Severi, M., Svensson, A., Vinther, B., Wolff,
665 E.W., 2013. The Antarctic ice core chronology (AICC2012): an optimized multi-parameter and multi-site
666 dating approach for the last 120 thousand years. 9, 1733-1748, doi:1710.5194/cp-1739-1733-2013.

667 WCRP-Coupled-Model-Intercomparison-Project-Phase-5, 2011. *CLIVAR Exchanges Newsletter special issue*
668 no 56, 16, no 2.

669 Wunch, 2002. What is the thermohaline circulation ? *Science* 298, 1179-1180.

670

1 **Table 1.** 130, 127 and 125 ka regional surface temperature changes deduced from the Capron et al. (2014) datasets and 129, 127 and 125 ka regional
2 surface temperature changes deduced from the Hoffman et al. (2017) datasets. Area-weighted average summer (or annual) SST values, calculated for
3 the North Atlantic and the Southern Ocean sectors and area-weighted annual air temperature values calculated for the Antarctic sector are indicated in
4 bold. For each case, the associated standard error (2σ) ranging 0.5 to 1.7°C is given in italics. The number of records considered for the calculation for
5 each sector and each time slice is indicated in brackets. A value and associated mean squared error is also given for regional surface temperature
6 differences between the (1) 127 and 130 ka and (2) 125 and 127 ka from the Capron et al. (2014) datasets. Details on the calculation methodology are
7 provided in the Supplementary Material.

	<i>Sector</i>	<i>130 a Mean 129 ka Mean</i>		<i>127 ka Mean</i>	<i>125 ka Mean 127-130 ka difference</i>	<i>125-127 ka difference</i>	
Capron et al. 2014 *	<i>N. Atl. Summer SST</i>	-4.2 ± 0.8 (13)	N/A	1.1 ± 0.7 (14)	1.2 ± 0.7 (14)	5.3 ± 1.0	0.1 ± 1.0
	<i>S. Ocean Summer SST</i>	1.8 ± 0.9 (15)	N/A	1.8 ± 0.8 (15)	1.6 ± 0.8 (15)	0.1 ± 1.2	-0.3 ± 1.2
	<i>Ant. Ann. Air Temp.</i>	1.9 ± 1.4 (4)	N/A	2.2 ± 1.4 (4)	1.3 ± 1.4 (4)	0.3 ± 2.0	-0.9 ± 2.0
Hoffman et al. 2017	<i>N. Atl. Summer SST</i>	N/A	-0.8 ± 1.7 (9)	1.9 ± 1.7 (9)	2.7 ± 1.2 (9)	N/A	N/A
	<i>N. Atl. Annual SST</i>	N/A	-3.0 ± 1.6 (9)	-0.2 ± 1.4 (9)	0.8 ± 1.0 (9)	N/A	N/A
	<i>S. Ocean Summer SST</i>	N/A	1.8 ± 1.0 (7)	1.6 ± 0.9 (7)	1.3 ± 1.0 (7)	N/A	N/A
	<i>S. Ocean Annual SST</i>	N/A	2.7 ± 1.0 (12) **	2.7 ± 1.0 (12) **	2.7 ± 1.1 (12) **	N/A	N/A

8 * Note that only marine sediment core records for which SST records are interpreted as summer signals are included in calculations from the Capron et al.
9 al. (2014) datasets. It results in considering all marine records (sites shown on Figure 2) except the DSDP-594 temperature record from the Southern
10 Ocean which is interpreted as an annual signal. All annual surface temperature reconstructions from the Antarctic ice core sites represented on Figure 2
11 have been included (4 records).

12 ** The Southern Ocean Annual SST average is anomalously high considering the Southern Ocean summer average (1.8 ± 0.9°C). This is likely due to high
13 SST anomalies calculated for cores ODP-1089, MD97-2121 and MD97-2120. For those three cores, HadISST preindustrial values are particularly low
14 compared to core top SST estimates, which could explain the high SST anomalies reconstructed at these sites.

15 **Table 2.** Strengths and limitations of the four most recent LIG surface temperature compilations (Turney and Jones, 2010; McKay et al., 2011; Capron et
 16 al., 2014; Hoffman et al., 2017).

	Climatic records	Geographical coverage	Time slice availability	Surface temperature anomaly averages and time period of reference	Record chronologies	Strengths	Limitations
Turney & Jones 2009	<ul style="list-style-type: none"> • 263 surface temperature records interpreted as annual signals; • SST from marine sediment cores based on Sr/Ca, unsaturated alkenone and Mg/Ca ratios, diatom and radiolarian transfer functions; • Surface air temperatures from polar ice cores based on water stable isotopes; • Surface air temperatures from terrestrial records based on pollen, macrofossil, coleptera. 	Global	<ul style="list-style-type: none"> • 1 map centered on LIG peak warmth: <ul style="list-style-type: none"> → Average across the benthic $\delta^{18}\text{O}$ plateau for marine records; → Average across the ice $\delta^{18}\text{O}$ plateau for ice records; → Average across “the period of maximum warmth” for terrestrial records. 	Peak warmth global annual average: <ul style="list-style-type: none"> • $+1.5 \pm 0.1^\circ\text{C}$ compared to 1961-1990); • $\sim +1.9^\circ\text{C}$ compared to <i>preindustrial</i> 	<ul style="list-style-type: none"> • Chronologies kept as in original publications of the records. 	<ul style="list-style-type: none"> • Global extent; • Largest spatial coverage; • Continental records are included. 	<ul style="list-style-type: none"> • No harmonized chronologies between records; • Peak-warmth centered map is not representative of any specific LIG time interval; • Global average not corrected for spatial coverage; • All SST records considered as annual signals; • Large uncertainties on Greenland maximum warmth estimates * • Lack of information on: <ul style="list-style-type: none"> → systematic quantitative surface temperature uncertainty estimates; → Calculation methodology of the global temperature average.

McKay et al. 2011	<ul style="list-style-type: none"> • 76 SST from marine sediment cores (Mg/Ca ratios in foraminifera, alkenone unsaturation ratios and faunal assemblage transfer functions (for radiolaria, foraminifera, diatoms and coccoliths); • Annual and summer SST signals; • Temporal resolution cut: < 3ka. 	Global ocean	<ul style="list-style-type: none"> • 1 map centered on LIG peak warmth calculated as the average SST of a 5 kyr period centered on the warmest temperature between 135 and 118 ka. 	<ul style="list-style-type: none"> • Peak LIG global SST: $+0.7 \pm 0.6^\circ\text{C}$ compared to <i>late Holocene</i>. 	<ul style="list-style-type: none"> • Chronologies kept as in original publications of the records. 	<ul style="list-style-type: none"> • Global ocean extent; • Global averages are ocean area-weighted (i.e. accounting for data sparseness) 	<ul style="list-style-type: none"> • No harmonized chronologies between records; • Peak-warmth centered map is not representative of any specific LIG time interval; • Limited to marine records
Capron et al. 2014; this study	<ul style="list-style-type: none"> • 42 marine sediment and 5 ice cores; • SAT from polar ice cores based on water stable isotopes; • 42 summer and 2 annual SST records based on $U^{K_{37}}$, planktonic foraminiferal Mg/Ca, macrofossil assemblage transfer functions of foraminifera, radiolarian and diatom assemblages, and percentage of polar foraminifera; • Temporal resolution cut: < 2 ka. 	Above 40°N and 40°S	<ul style="list-style-type: none"> • 115, 120, 125, 127, 130 ka time slices; They are calculated as the median value of interpolated temperature across a 2 ka time window centered on the given value. 	<ul style="list-style-type: none"> • Ocean area-weighted averages for the North Atlantic, Southern Ocean and Antarctica (see Table 1); • 1870-1899 climatology (this study); • WOA 98 (Capron et al. 2014). 	<ul style="list-style-type: none"> • Common temporal framework build for marine and ice records; • AICC2012 as a reference age scale (Bazin et al. 2012; Veres et al. 2012); • Calculation of surface temperature on age scale and associated uncertainty based on linear interpolation and Monte Carlo analysis. 	<ul style="list-style-type: none"> • Harmonized chronologies; • Uncertainty estimate through Monte-Carlo simulations; • Time series between 110 and 135 ka and associated with 2σ uncertainties; • Ocean area-weighted regional averages; • Includes polar ice cores. 	<ul style="list-style-type: none"> • Spatial coverage limited to high latitude regions; • Does not include terrestrial records; • Relative uncertainty attached to age markers estimated visually.

Hoffman et al. 2017	<ul style="list-style-type: none"> • 83 marine sediment cores • SST based on U^{K}_{37}, planktonic foraminiferal Mg/Ca and microfossil assemblage transfer function (foraminifera, radiolarian, coccoliths, diatoms); • Temporal resolution cut: < 4 ka 	Global ocean	<ul style="list-style-type: none"> • 120, 125 and 129 ka maps; • Global and regional temporal stacks between 115 and 130 ka; • Corresponding surface temperature taken at the given value from the 0.1 ka interpolated timeseries. 	• 1870-1889 climatology	<ul style="list-style-type: none"> • Common temporal framework built for marine records; • SpeleoAge as a reference age scale (Barker et al. 2011); • SST on age scale and associated quantitative uncertainties deduced from Bayesian statistics and Monte Carlo Analysis 	<ul style="list-style-type: none"> • Harmonized chronologies; • Uncertainty estimates through Monte-Carlo simulations; • Method to calculate age models based on Bayesian statistics; • Interpolated time series between 130 and 115 ka and associated 2σ uncertainties. • Global and regional stacks with 2σ uncertainties; • Ocean area-weighted global averages. 	<ul style="list-style-type: none"> • Does not include ice and terrestrial records; • Limitations associated with the use of global relationships to infer SST from Mg/Ca from planktonic foraminifera and from alkenone ratio. • Despite a correction attempt, potential bias linked to the calculation of annual SST from the combination of summer and winter SST estimates.
---------------------	---	--------------	---	-------------------------	---	---	---

17 * The GRIP ice core is affected by ice mixing near the bedrock preventing a robust dating of the LIG layers and the identification of the LIG maximum
18 warmth (Johnsen et al. 1992). The NorthGRIP ice core unlikely records the LIG maximum warmth as it provides a continuous climatic record extending
19 back to about 123 ka (NorthGRIP project members 2004).

20 **Table 3.** Quantitative surface temperature differences between the different LIG syntheses for marine sites included in our synthesis and at least one of
21 the other syntheses from Turney and Jones (2010), McKay et al. (2011) and Hoffman et al. (2017).
22 At the bottom of the table and for each column, the Root Mean Squared deviation (RMSD) is calculated considering (1) only North Atlantic sites, (2) only
23 Southern Ocean sites and (3) all sites. Sites in italics are sites whose SST records are interpreted as annual signals in the Capron et al. (2014)
24 compilation.

	Core	Latitude	Longitude	Temp. dif. [T&J Peak warmth vs. 127ka SST anomaly relative to PI] *	Temp. dif. [McKay peak warmth vs 127ka summer SST anomaly relative to PI] **	Temp. dif. [Hoffman 127 ka summer SST vs this study's 127 ka summer SST] ***
North Atlantic	EW9302-JPC8	61.0	-25.0	-2.5		-2.0
	ODP 980	55.8	-14.1	2.8		-0.2
	NA87-25	55.6	-14.8			0.0
	M23414-9	53.5	-20.3	-1.6	-0.7	
	NEAP18K	53.0	-30.0			1.0
	K708-1	50.0	-23.7	8.9	-0.2	
	SU90-08	43.4	-30.4	-1.2		
	CH69-K09	41.8	-47.4			-1.0
	V30-97	41.0	-32.9	0.5	3.9	
	SU90-03	40.5	-32.0			-1.6
Southern Ocean	MD97-2121	-40.2	177.6	-2.8	-0.9	
	ODP1089	-40.9	9.9		-2.2	-1.1
	MD94-101	-42.5	79.4			0.1
	PS2489-2	-42.5	8.6		1.4	-0.4
	MD94-102	-43.5	79.8			0.3
	DSDP-594	-45.3	174.6	-0.3	-1.5	
	MD97-2120	-45.5	174.9	2.6	1.0	
	MD88-770	-46.0	96.5	0.1		-1.4
	MD02-2488	-46.5	88.0			-0.1
	SO136-111	-56.4	160.1		0.3	
RMSD (North Atlantic sites only)				4.0	2.3	1.2
RMSD (Southern Ocean sites only)				1.9	1.4	0.8
RMSD (All sites)				3.4	1.7	1.1

25

26 * Difference between the LIG peak warmth anomaly relative to the 1961-1990 Mean from Turney and Jones (2010) and the 127 ka surface temperature
27 anomaly relative to the 1870-1899 mean (this study);

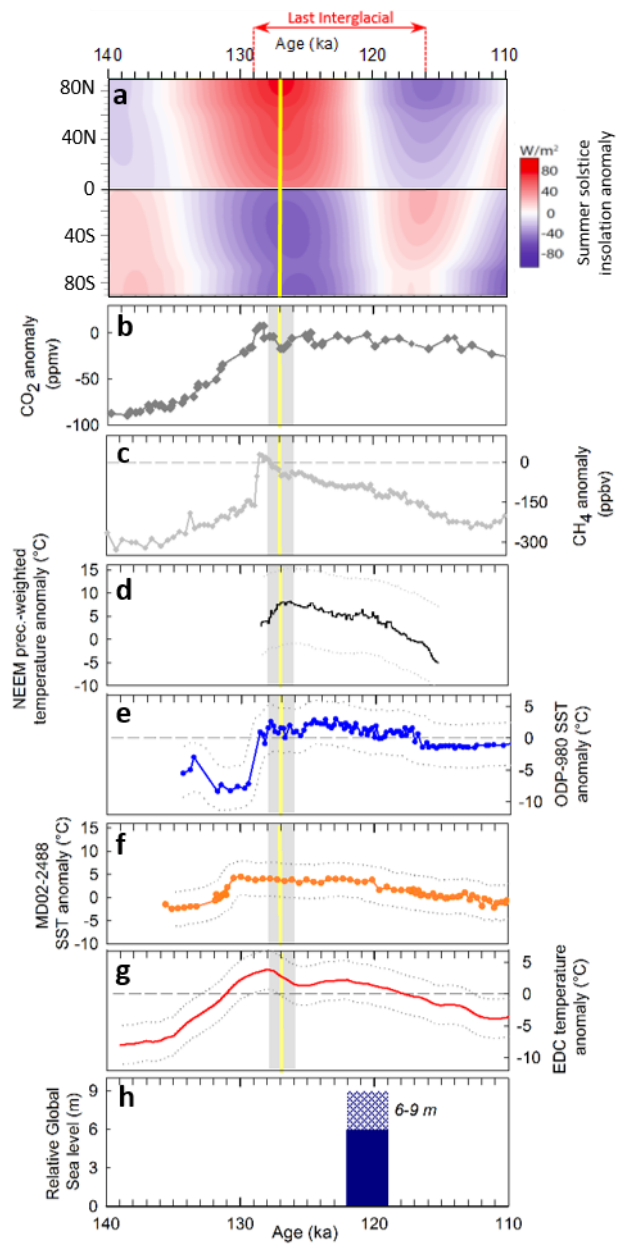
28 ** Difference between the LIG peak warmth anomaly relative to the late Holocene from McKay et al. (2011) and the 127 ka surface temperature
29 anomaly relative to the 1870-1899 mean (this study);

30 *** Difference between the 127 ka value from Hoffman et al. (2017) and the 127 ka surface temperature from this study. Note that in this case we only
31 consider sites with identical seasonal interpretation in both the Hoffman et al. (2017) and Capron et al. (2014) syntheses.

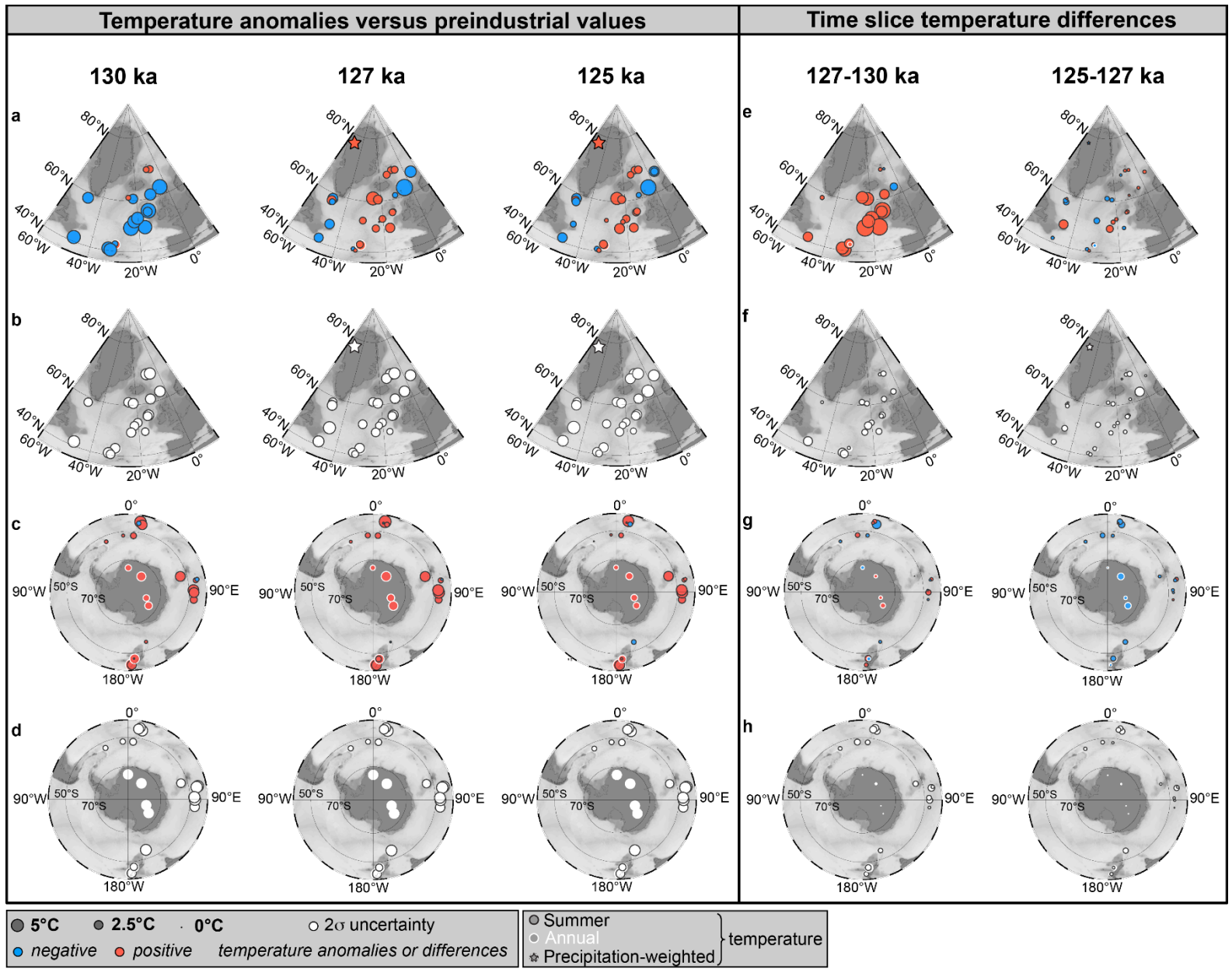
1 **Figure 1.** Forcing and climatic records across the 110-140 ka time interval. The LIG time interval is indicated by the red vertical dotted lines and
2 horizontal arrow between 129 and 116 ka following the definition based on the eustatic sea level (Masson-Delmotte et al., 2013). Records are displayed
3 in panels **a), b), c), d)** and **g)** as anomalies relative to the average value of the last 1000 years. As for the two marine records displayed in **e)** and **f)**, the
4 reference summer SST are taken from the World Ocean Atlas 1998 (10m-depth; Capron et al., 2014).

5 **a)** 21st June across the Northern Hemisphere and 21st December insolation across the Southern Hemisphere respectively;
6 **b)** Atmospheric CO₂ concentration (Lüthi et al., 2008);
7 **c)** Atmospheric CH₄ concentration (Loulergue et al., 2008);
8 **d)** Greenland NEEM precipitation-weighted temperature reconstruction, (NEEM community members 2012) and associated 2 σ uncertainty envelope
9 (dotted lines, this study);
10 **e)** North Atlantic marine core ODP 980 summer SST reconstruction (Oppo et al., 2006) and associated 2 σ uncertainty envelope (dotted line; Capron et
11 al. 2014);
12 **f)** Southern Ocean marine core MD02-2488 SST summer reconstruction (Govin et al., 2012) and associated 2 σ uncertainty envelope (dotted lines;
13 Capron et al., 2014);
14 **g)** Antarctic EDC annual surface air temperature reconstruction (Masson-Delmotte et al., 2011) and associated 2 σ uncertainty envelope (dotted line;
15 this study).
16 **h)** Maximum global mean sea level (GMSL) relative to present-day, uncertainties remain both in the amplitude (6 to 9 m; indicated by the shading) and
17 in the exact timing of the LIG GMSL peak. However, most studies point toward a late LIG GMSL peak occurring between 119 and 122 ka (see Dutton et
18 al., 2015 for a review).

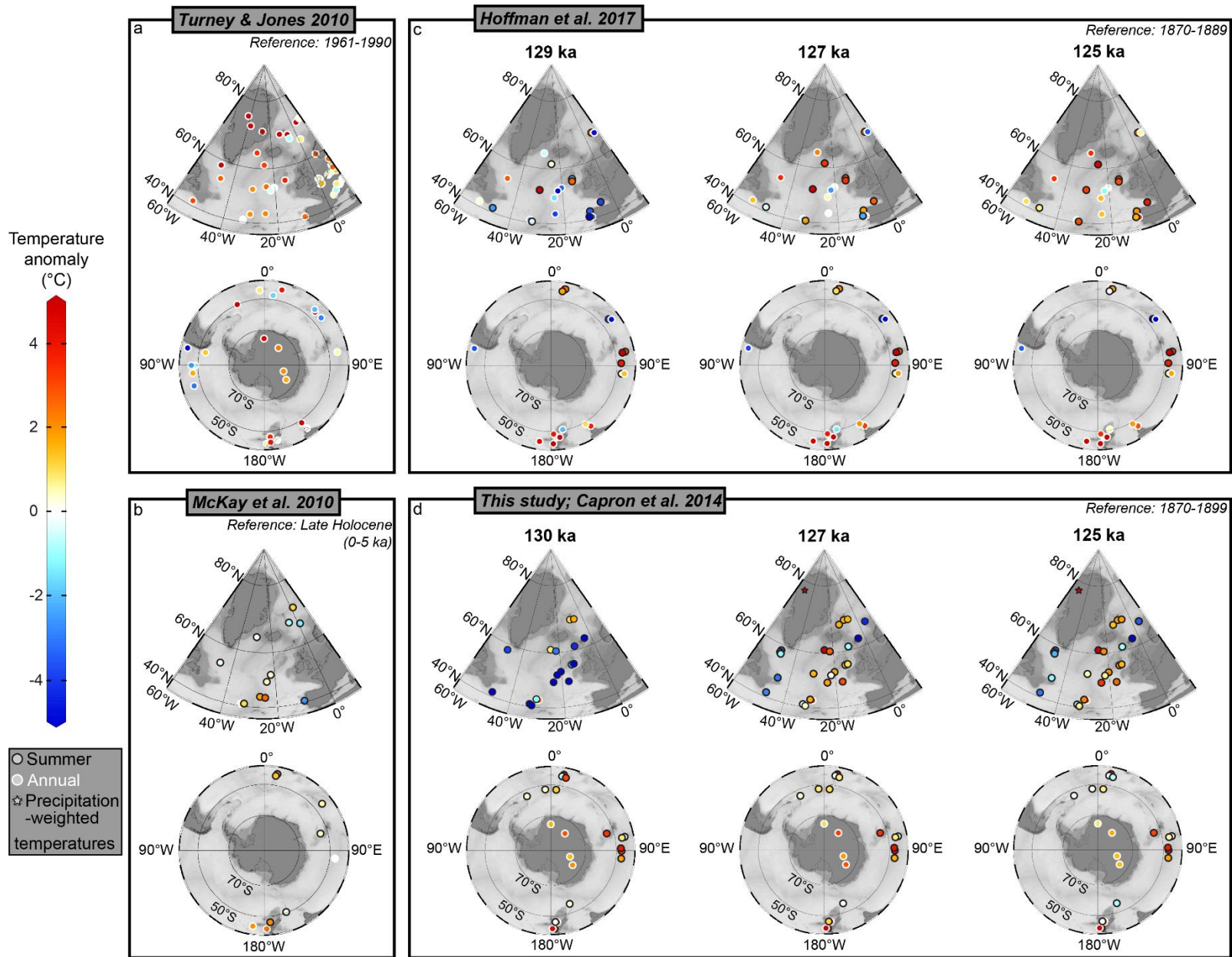
19 Records on panels **b** to **g** are displayed on the AICC2012 chronology (Bazin et al., 2012; Veres et al., 2012; Capron et al., 2014). 2 σ envelopes associated
20 with surface temperature records on panels **d** to **g** account both for the relative dating and temperature tracer uncertainties. The vertical yellow line
21 indicates 127 ka, the time interval chosen to run the coordinated CMIP6/PMIP4 LIG Tier 1 and Tier 2 simulations. The grey shading indicates the 126-
22 128 ka time interval used to build the climate data-based 127 ka time slice.



24 **Figure 2. LIG temperature anomalies obtained from the Capron et al. 2014 compilation.**
25 Left panel: Air temperature and SST anomalies **(a, c)** calculated relative to preindustrial and associated 2σ uncertainties of temperature anomalies **(b,**
26 **d)** at 130 ka (left), 127 ka (middle) and 125 ka (right) obtained in the Northern Hemisphere **(a, b)** and the Southern Hemisphere **(c, d)**.
27 Right panel: Temperature differences **(e, g)** and associated 2σ uncertainties **(f, h)** between the 127 and 130 ka time slices (left) and between the 125
28 and 127 ka time slices (right) in the Northern Hemisphere **(e, f)** and the Southern Hemisphere **(g, h)**. The bigger the dot is, the larger the anomaly **(a, b)**
29 and the uncertainty **(c, d)** are. Warming (cooling) versus preindustrial temperature is represented in red (blue). Black circles indicate summer signals,
30 white circles indicate annual signals and the star indicates the Greenland site whose temperature record is interpreted as a precipitation-weighted
31 signal (NEEM community members, 2012).
32 Values for the 130 and 125 ka SST anomalies and associated 2σ errors are identical to the ones provided by Capron et al. (2014) but some differences
33 exist regarding the 130 and 125 ka surface air temperature estimates and associated uncertainties for reasons described in Section 2.



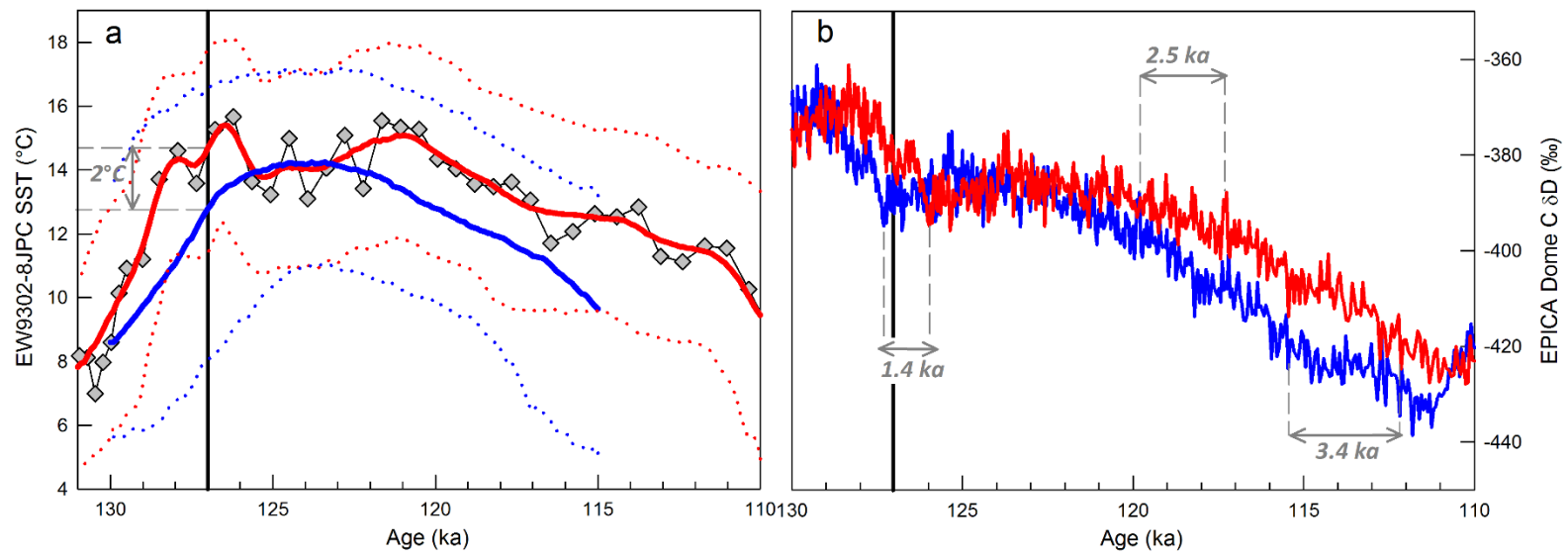
35 **Figure 3.** Comparison of four existing LIG surface temperature syntheses in the high latitude regions (poleward of latitude 40°N/S).
36 **a)** The Turney and Jones (2010) synthesis of LIG peak surface warmth relative to the 1961-1990 mean, including reconstructions from terrestrial,
37 marine and ice records and all interpreted as annual signals (white circle);
38 **b)** The McKay et al. (2011) synthesis of LIG peak warmth relative to the Late Holocene (last 5 ka), including marine records interpreted as summer
39 (black circle) or annual signals (white circle), following the information given for each core in the supplementary material of McKay et al., 2011);
40 **c)** 129, 127 and 125 ka time slices of surface temperature anomaly relative to Preindustrial (1870-1889) including marine records interpreted as
41 summer or annual signals from Hoffman et al. (2017). See Section 4.1.2 for details on the calculation of the 127 ka based on the Hoffman et al. (2017)
42 synthesis.
43 **d)** 130, 127 and 125 ka time slices of surface temperature anomaly relative to Preindustrial (1870-1899), including ice and marine records based on the
44 Capron et al. (2014) synthesis.
45



47 **Figure 4.** Illustrating the differences resulting from the use of different age methodologies and of different reference time scales as described in Capron
48 et al. (2014) and in Hoffman et al. (2014). The North Atlantic core EW9302-8JPC SST record is used as a case study (Oppo et al., 1997; Oppo et al., 2001).
49 Note that both compilations use the same raw SST dataset on a depth scale.

50 **a)** The black curve with grey diamonds represents the raw EW9302-8JPC SST data displayed on AICC2012 (Bazin et al., 2012; Veres et al., 2012). The
51 SST data are transferred onto an age scale based on a linear interpolation between the age markers defined by Capron et al. (2014). The thick red line
52 represents the median 100 year-interpolated record and associated non-parametric 2σ (2.5th and 97.5th percentiles, dotted red lines) confidence
53 intervals resulting from the 1000 Monte Carlo iterations (methodology described in Section 2 and Capron et al., 2014). The thick blue line represents
54 the mean 100 year-interpolated curve presented on the Asian speleothem-based EDC3 chronology (Barker et al., 2011) as reference age model, and
55 defined using Bchron, a Bayesian age-depth modeling routine (Haslett & Parnell, 2008) to propagate age and tracer uncertainties. These different
56 methodologies explain the 2°C offset obtained at 127 ka (vertical black line) between the red and blue curves.

57 **b)** EPICA Dome C water isotopic profile (Jouzel et al., 2007) displayed on the AICC2012 timescale in red and on the SpeleoAge timescale in blue.
58 Horizontal grey arrows indicate the age difference in specific events between the two age scales. An age difference of about 1.4 ka prevails between the
59 two timescales at 127 ka. Age differences around 120 and 115 ka illustrate that the choice of a reference timescale becomes increasingly critical at the
60 end of the LIG and over the glacial inception when an offset of more than 3 ka is observed between the two time scales around 115 ka.
61 In both panels, the vertical black line indicates the 127 ka time interval.



62